New Trends in the Chemistry of Iron(III) Citrate Complexes: Correlations between X-ray Structures and Solution Species Probed by Electrospray Mass Spectrometry and Kinetics of Iron Uptake from Citrate by Iron Chelators

Isabelle Gautier-Luneau,*[a, c] Claire Merle,[a] Delphine Phanon,[a, c] Colette Lebrun,[b] Frédéric Biaso,[a] Guy Serratrice,[a] and Jean-Louis Pierre[a]

Abstract: Despite the crucial role of "iron(III) citrate systems" in the iron metabolism of living organisms (bacteria as well as plants or mammals), the coordination chemistry of ferric citrate remains poorly defined. Variations in the experimental conditions used for the preparation of so-called ferric citrates (iron salt, Fe:cit molar ratio, base, pH, temperature, solvent) lead to several different species, which are in equilibrium in solution. To date, six different anionic complexes have been structurally characterized in the solid state, by ourselves or others. In the work described herein, we have established the experimental conditions leading to each of them. Five were obtained from aqueous solution. With the exception of a nonanuclear species (of which fragments have been detected), all were identified in aqueous solution on the basis of electrospray ionization mass spectrometry. In addition, the spectra revealed a new trinuclear species, which could not be crystallized. Kinetic studies of iron uptake from citrate species by iron chelators confirmed the results indicated by the ESI-MS studies. These studies also allowed the relative molar fraction of mononuclear versus polynuclear complexes to be determined, which depends on the Fe:cit molar ratio.

Keywords: citrate ligands · electrospray mass spectrometry · iron · kinetics · solid-state structures

Introduction

Citric acid is ubiquitous in Nature and it has key biological functions.[1] The tricarboxylic acid and its salts are used in a wide variety of industrial applications (e.g., in soft drinks and effervescent salts, as an antioxidant in foods, as a sequestering agent for metal ions, as a cleaning and polishing agent for metals, as a mordant in dyeing). Most of these applications arise from the affinity of citrate for metal ions. In plants, citric acid is present in root exudates, where it serves to depolymerize and solubilize ferric hydroxide in soil and to mobilize the iron to the membranes of the root cells.[2] Citrate is also used to transport ferric iron to leaves as a constituent of xylem sap, and a link between iron metabolism and citrate concentration in plants has been established.[3] Citrate is not formed by bacteria, but it can act as an exogenous siderophore (*Escherichia coli* possesses a transport system which is specific for ferric citrate).[4] In animals (including humans), citrate, which occurs in blood plasma at about 0.1 mM, promotes the bioavailability of dietary non-heme iron.[5]

Our interest in iron complexation and in iron metabolism[6] led us to study iron(III) citrate systems. To date, the coordination chemistry of ferric citrates remains rather poorly defined.[7] By varying the experimental conditions used for the preparation of the so-called ferric citrates (the iron salt used; the iron(III):citric acid (H_4cit) molar ratio, de-

[a] Prof. I. Gautier-Luneau, C. Merle, D. Phanon, Dr. F. Biaso, Prof. G. Serratrice, Prof. J.-L. Pierre
Laboratoire de Chimie Biomimétique, LEDSS, ICMG, UMR CNRS 5616, Université Joseph Fourier
BP 53, 38041 Grenoble Cedex 9 (France)
E-mail: isabelle.gautier-luneau@grenoble.cnrs.fr

[b] C. Lebrun
Laboratoire de Reconnaissance ionique/DRFMC/SCIB/CEA Grenoble, 17 avenue des Martyrs, 38054 Grenoble Cedex 9 (France)

[c] Prof. I. Gautier-Luneau, D. Phanon
Present address: Laboratoire de Cristallographie, CNRS, 25 avenue des Martyrs, BP 166, 38042 Grenoble Cedex 9 (France)
Fax: (+33) 4 76 88 10 38

Supporting information for this article is available on the WWW under http://www.chemeurj.org/or from the author: selected interatomic distances and bond angles in compounds **1**–**8**; an ORTEP representation of the anionic complex in compound **8**; ESI mass spectra; chemical formulae of O-TRENSOX and TREMCAMS; rate constant data.

 DOI: 10.1002/chem.200401087

noted herein as Fe:cit ratio; the added base, as well as pH, temperature, and solvent), different species can be obtained, which may be in equilibrium in solution. Spiro et al.[8] have found evidence for the formation of polynuclear aggregates. Citrate chelates iron(III) ions at equimolar concentration and low pH, with the loss of the alcoholic hydroxyl proton, but upon neutralization of the solution polymeric iron hydroxides are produced. On the other hand, an excess of citrate can provide a protective coating and prevent polymerization. Two studies performed in aqueous solutions at up to pH 4 have yielded conflicting results![9,10] The monoferric dicitrate $[Fe(H_xcit)_2]^{(5-2x)-}$ species has been claimed to be recognized by the *E. coli* transport system, and indeed seems to be the only complex of established biological relevance.[11] The $[Fe(cit)_2]^{5-}$ species has been structurally characterized (crystallized from solution at pH 8) by Matzapetakis et al.[12] The "recognition" of the mononuclear dicitrate species may be questioned in the light of recent papers describing the crystallographic structure of FecA, the outer membrane receptor of the citrate system of *E. coli*, which binds a dinuclear ferric dicitrate.[13] The X-ray structure of such an $[Fe_2(cit)_2(H_2O)_2]^{2-}$ diferric dicitrate complex has been determined by Shewky et al., along with that of the species $[Fe_2(Hcit)_3]^{3-}$.[14] These dinuclear complexes were obtained in the presence of pyridine and neocuproine, respectively, the protonated forms of these bases acting as the counter-cations in the complexes. The authors suggest that the two complexes are in equilibrium in aqueous solution, and that one or other of them crystallizes according to the base used. The structure of a nonairon(III) complex, $[Fe_9O(cit)_8(H_2O)_3]^{7-}$, which comprises of three trinuclear subunits, has also been described by Bino et al.[15]

Herein, we report on the synthesis and characterization of dinuclear and mononuclear complexes, and on a systematic study of the effect of varying the synthetic conditions, namely the iron salt used (perchlorate, chloride or nitrate), the added base (imidazole, picoline, pyridine, neocuproine or ammonium hydroxide), the pH, the Fe:cit ratio, the solvent (water or DMF), and the temperature. We have established the experimental conditions leading to each respective complex, and we present for the first time some correlations between the X-ray structures and the species in solution, as probed by electrospray mass spectrometry and kinetics. Two kinds of solutions were analyzed by ESI-MS: 1) the final solutions, from which different compounds had been crystallized, to compare the species obtained in the solid state with those present in solution; 2) a series of solutions at different Fe:cit ratios and pH to monitor the evolution of the speciation. Furthermore, we describe a series of kinetic measurements of the iron uptake from citrate complexes at physiological pH 7.4 by two tripodal chelators: the tris(8-hydroxyquinolinate) ligand O-TRENSOX[16] and the tris(catecholate) ligand TRENCAMS.[17] These kinetic measurements were used to provide insight into the speciation between mononuclear and polynuclear Fe citrate species in relation to the Fe:cit ratio. These species could be distinguished on the basis of their kinetic abilities to transfer iron to a given chelator: the mononuclear complex is expected to be more reactive than the polynuclear complexes, having coordination sites more accessible to an incoming chelator.

Experimental Section

Syntheses: Compounds **1**–**5**, with the general formula $(Hbase)_2[Fe_2(cit)_2(H_2O)_2]\cdot n H_2O$, were synthesized by using various bases (pyridine (py), imidazole (im), picoline (pic), or neocuproine (neo)) and different ferric salts (perchlorate, chloride or nitrate). They were prepared by first stirring citric acid, the ferric salt, and the base at appropriate concentrations at room temperature. In the case of compounds **1**–**4**, yellow-green platelet crystals were obtained by slow evaporation of the water from the aqueous reaction mixture protected from light. The pH of the solutions was found to be between 2.2 and 3.5. In the case of pyridine and imidazole, different solutions corresponding to different ferric salt:citric acid (Fe:cit) molar ratios were prepared in water or in DMF. Compounds **5** and **6** were successively obtained at room temperature by slow evaporation of the volatiles from a solution that had been previously heated at 60 °C for 30 min. Compounds **7** and **8**, which are monoferric dicitrate species, were also successively obtained by evaporation of the volatiles from the same solution. For elemental analysis, crystals were collected by filtration, washed with ethanol, and dried under vacuum.

$(Hpy)_2[Fe_2(cit)_2(H_2O)_2]\cdot 2H_2O$ (1): This compound was previously obtained by Shweky et al.[14] from an aqueous solution containing equimolar amounts of $Fe(NO_3)_3\cdot 2H_2O/Na_3Hcit/py$. We obtained the same compound under various conditions, that is, from an aqueous solution (in the pH range 2.2–3.5) of $FeCl_3\cdot 6H_2O/H_4cit/py$ with a molar ratio of 3:1:2, and also when using the nitrate and the perchlorate salts in molar ratios of 1:1:4 and 1:4:6, respectively. We also obtained this compound from a solution in DMF, starting from $Fe(ClO_4)_3\cdot 9H_2O/H_4cit/py$ in a molar ratio of 1:1:4.

$(Him)_2[Fe_2(cit)_2(H_2O)_2]\cdot 2H_2O$ (2): Single crystals suitable for X-ray diffraction analysis were obtained from a solution at pH 2.8 containing $Fe(NO_3)_3\cdot 6H_2O/H_4cit/im$ in a molar ratio of 1:1:4. Elemental analysis calcd (%) for $C_{18}H_{22}N_4O_{16}Fe_2\cdot 2H_2O$: C 30.97, H 3.75, N 8.03, Fe 15.99; found C 31.01, H 3.82, N 7.85, Fe 15.83.

The same compound, as characterized by measurement of the cell parameters for a single crystal and/or elemental analysis, was also obtained by starting from $Fe(ClO_4)_3\cdot 9H_2O/H_4cit/im$ in a molar ratio of 1:1:4 or 1:2:6.

The compound $(Him)_2[Fe_2(cit)_2(H_2O)_2]\cdot H_2O\cdot DMF$ was obtained from a solution in DMF containing $Fe(ClO_4)_3\cdot 9H_2O/H_4cit/im$ in a molar ratio of 1:1:4. Elemental analysis calcd (%) for $C_{18}H_{22}N_4O_{16}Fe_2\cdot H_2O\cdot C_3H_7NO$: C 33.49, H 4.15, N 9.30, Fe 14.83; found: C 33.88, H 4.16, N 9.33, Fe 15.00.

$(Hpic)_2[Fe_2(cit)_2(H_2O)_2]\cdot 6H_2O$ (3): Single crystals suitable for X-ray diffraction analysis were obtained from an aqueous solution (pH 2.9) containing $Fe(ClO_4)_3\cdot 9H_2O/H_4cit/pic$ in a molar ratio of 1:1:4. Elemental analysis calcd (%) for $C_{24}H_{28}N_2O_{16}Fe_2\cdot 6H_2O$: C 35.14, H 4.92, N 3.42, Fe 13.62; found: C 35.05, H 4.90, N 3.32, Fe 13.83.

α-$(Hneo)_2[Fe_2(cit)_2(H_2O)_2]\cdot 8H_2O$ (4): Single crystals suitable for X-ray diffraction analysis were obtained from an aqueous solution (pH 2.6) containing $Fe(NO_3)_3\cdot 6H_2O/H_4cit/neo$ in a molar ratio of 1:1:4. Elemental analysis calcd (%) for $C_{40}H_{38}N_4O_{16}Fe_2\cdot 8H_2O$: C 44.22, H 5.01, N 5.16, Fe 10.28; found: C 44.44, H 5.01, N 5.29, Fe 9.87.

β-$(Hneo)_2[Fe_2(cit)_2(H_2O)_2]\cdot 8H_2O$ (5): A solution of the composition described for the preparation of compound **4** was heated at 60 °C for 30 min, as described by Bino et al.[15] Colorless needles of neocuproinium nitrate crystallized from the brown-yellow solution at room temperature, which were removed by filtration. After a day, colorless crystals and small orange crystals had separated from the filtrate. The latter corresponded to $(Hneo)_7[Fe_9O(cit)_8(H_2O)_3]\cdot neo\cdot 61H_2O$, as previously characterized by Bino et al.[15] After four days, without filtration, yellow platelets crystallized from the same solution. X-ray analysis revealed that they consisted of a compound with the same chemical formula as compound

4, $(Hneo)_2[Fe_2(cit)_2(H_2O)_2]\cdot 8H_2O$, but with a different crystal packing; the forms are denoted α and β.

$(Hneo)_3[Fe_2(Hcit)_3]\cdot 8H_2O$ (6): After two weeks, this compound crystallized in the form of block-shaped crystals as the fourth species from the same solution that had yielded compound **5**. The final pH of the solution was 1.5. A green crystal was cut and subjected to XRD measurements. Compounds with the formula $(Hneo)_3[Fe_2(Hcit)_3]\cdot n H_2O$ ($n = 8$ and $n = 14$) were previously obtained and characterized by Bino et al.[15] from an aqueous solution of $[Fe_3O(O_2CCH_3)_6(H_2O)_3](NO_3)$/$H_4$cit/neo in a molar ratio of 1:4.3:4.6.

We also obtained the compound $(Hneo)_3[Fe_2(Hcit)_3]\cdot 14H_2O$, which crystallized directly from an aqueous solution of $Fe(NO_3)_3\cdot 6H_2O$/H_4cit/neo in a molar ratio of 1:4:3 at pH 1.8 after heating to 60 °C. It was characterized by measurement of the cell parameters for a single crystal and by elemental analysis, and was found to correspond to the trihydrate after the crystals had been dried in vacuo. Elemental analysis calcd (%) for $C_{60}H_{54}N_6O_{21}Fe_2\cdot 3H_2O$: C 52.96, H 4.44, N 6.18, Fe 8.21; found: C 52.97, H 4.49, N 6.24, Fe 7.47.

$(NH_4)_5[Fe(cit)_2]\cdot 2H_2O$ (7): The pH of an aqueous solution containing $Fe(NO_3)_3\cdot 6H_2O$/H_4cit/py in a molar ratio of 1:4:5 was adjusted to 7.1 by adding aqueous ammonia solution with stirring. Yellow parallelepiped crystals suitable for X-ray diffraction analysis were obtained after one month by slow evaporation of the solvent from this aqueous solution. This compound had previously been prepared at pH 8 and characterized by Matzapetakis et al.[12]

$(NH_4)_4[Fe(Hcit)(cit)]\cdot 3H_2O$ (8): After a further two weeks of evaporation of the volatiles from the previous solution containing crystals of compound **7**, yellow block-shaped crystals were obtained. The final pH of the solution was 6. This compound was also obtained directly by concentration of a solution at pH 6.

X-ray data collection and crystal structure determination: Crystal data, together with details of the diffraction experiments and the refinement procedures, are summarized in Table 1 and Table 2. All crystals of compounds **1**–**6** were enclosed in capillary tubes and mounted on an Enraf-Nonius CAD4 diffractometer; they were examined by using graphite-monochromated radiation ($\lambda(Mo_{K\alpha}) = 0.71073$ Å) at 293 K. Crystals of compounds **7** and **8** were mounted on a Kappa CCD Nonius diffractometer and examined with graphite-monochromated $Mo_{K\alpha}$ radiation ($\lambda = 0.71073$ Å) at 170 K. The reflections were corrected for Lorentz and polarization effects but not for absorption. All structures were solved by direct methods and refined by using TEXSAN software.[18] All non-hydrogen atoms were refined with anisotropic thermal parameters. Hydrogen atoms were located on a difference Fourier map, and were treated as riding on their carrier atoms, with isotropic thermal parameters. The refinement of the crystal structure of compound **7** requires some comments. $(NH_4)_5[Fe(cit)_2]\cdot 2H_2O$ crystallizes in the triclinic space group $P\bar{1}$. The mononuclear complex is centrosymmetric with the iron atom localized at an inversion center. The asymmetric unit was found to comprise 0.5 Fe^{III}, 1 cit^{4-}, 2.5 NH_4^+, and 1 H_2O. At first glance, one might be tempted to place two ammonium nitrogen atoms and one water oxygen atom at general positions and one ammonium nitrogen atom at a special position (inversion center) with a site occupancy factor (s.o.f.) of 0.5. Doing so, the symmetry expansion of two hydrogen atoms linked to this nitrogen would lead to a non-consistent square-planar ammonium cation. In the previously reported structure[12] of **7**, and also for the isostructural compounds $(NH_4)_5[Al(cit)_2]\cdot 2H_2O$, $(NH_4)_5[Ga(cit)_2]\cdot 2H_2O$, and $(NH_4)_5[Mn(cit)_2]\cdot 2H_2O$,[19,20] the authors suggested that this ammonium cation was disordered. As has been underlined in a study of aluminum and gallium citrate complexes,[19b] the nitrogen and oxygen atoms have almost the same weights in the Fourier map. Thus, these atoms must be carefully assigned. During the refinement of the structure of compound **7**, anisotropic refinement of the difference Fourier map around the water oxygen atom (in a general position as in ref. [12] and ref. [19]) revealed four peaks (Q1, Q4, Q16, and Q19) attributable to hydrogen atoms in a tetrahedral geometry. The ammonium nitrogen (N3) atom and the water

Table 2. Crystal data of compounds **6**–**8**.

Compound	**6**[c]	**7**	**8**
formula	$(Hneo)_3[Fe_2(Hcit)_3]\cdot 8H_2O$	$(NH_4)_5[Fe(cit)_2]\cdot 2H_2O$	$(NH_4)_4[Fe(Hcit)(cit)]\cdot 3H_2O$
	$Fe_2C_{60}H_{70}N_6O_{29}$	$FeC_{12}H_{32}N_5O_{16}$	$FeC_{12}H_{31}N_4O_{17}$
FW [g mol^{-1}]	1450.93	558.26	554.24
crystal system	triclinic	triclinic	monoclinic
space group	$P\bar{1}$	$P\bar{1}$	$C2/c$
a [Å]	12.882(4)	7.239(1)	27.226(3)
b [Å]	12.821(3)	9.547(1)	10.011(1)
c [Å]	20.614(3)	9.619(1)	19.133(2)
α [°]	101.76(2)	118.45(1)	90
β [°]	102.94(2)	91.16(1)	122.79(1)
γ [°]	86.49(2)	105.73(1)	90
V [Å^3]/Z	3248(2)/2	553.8(2)/1	4383.9(9)/8
ρ_{calcd} [g cm^{-3}]	1.483	1.674	1.694
crystal dimensions [mm]		$0.2\times0.2\times0.35$	$0.15\times0.2\times0.2$
$R(F)$[a]		0.0389	0.0406
$R_w(F)$[b]		0.0593	0.0464
goodness of fit S		1.96	1.84

[a] $R = \Sigma||F_o|-|F_c||/\Sigma|F_o|$. [b] $R_w = [\Sigma(|F_o|-|F_c|)^2/\Sigma wF_o^2]^{1/2}$ with $w = 1/[\sigma^2(F_o) + p|F_o|^2]$. [c] From reference [14].

Table 1. Crystal data of compounds **1**–**5** of the general formula $(Hbase)_2[Fe_2(cit)_2(H_2O)_2]\cdot n H_2O$.

Compound	**1**[c]	**2**	**3**	**4**	**5**
formula	$(Hpy)_2[Fe_2(cit)_2(H_2O)_2]\cdot 2H_2O$	$(Him)_2[Fe_2(cit)_2(H_2O)_2]\cdot 2H_2O$	$(Hpic)_2[Fe_2(cit)_2(H_2O)_2]\cdot 6H_2O$	α-$(Hneo)_2[Fe_2(cit)_2(H_2O)_2]\cdot 8H_2O$	β-$(Hneo)_2[Fe_2(cit)_2(H_2O)_2]\cdot 8H_2O$
	$Fe_2C_{22}H_{28}N_2O_{18}$	$Fe_2C_{18}H_{26}N_4O_{18}$	$Fe_2C_{24}H_{40}N_2O_{22}$	$Fe_2C_{40}H_{54}N_4O_{24}$	$Fe_2C_{40}H_{54}N_4O_{24}$
FW [g mol^{-1}]	720.14	698.10	820.28	1086.58	1086.58
crystal system	triclinic	triclinic	triclinic	triclinic	triclinic
space group	$P\bar{1}$	$P\bar{1}$	$P\bar{1}$	$P\bar{1}$	$P\bar{1}$
a [Å]	8.711(3)	8.712(1)	8.047(2)	7.137(6)	6.790(10)
b [Å]	11.262(3)	10.677(2)	10.678(2)	10.871(3)	10.725(3)
c [Å]	7.768(3)	7.650(1)	10.871(2)	15.134(6)	15.924(4)
α [°]	109.32(2)	106.13(2)	111.14(2)	93.21(2)	89.84(2)
β [°]	105.85(2)	74.29(1)	90.86(2)	92.03(6)	98.79(6)
γ [°]	84.51(2)	97.11(1)	87.64(2)	95.24(4)	98.02(6)
V [Å^3]/Z	691.3(2)/1	657.1(2)/1	870.5(3)/1	1166(1)/1	1134(1)/1
ρ_{calcd} [g cm^{-3}]	1.745	1.764	1.565	1.547	1.591
crystal dimensions [mm]		$0.2\times0.2\times0.1$	$0.3\times0.2\times0.2$	$0.3\times0.3\times0.2$	$0.3\times0.25\times0.1$
$R(F)$[a]/$R_w(F)$[b]		0.0386/0.0463	0.0473/0.0353	0.0412/0.0632	0.0424/0.0553
goodness of fit S		1.87	1.24	1.44	1.91

[a] $R = \Sigma||F_o|-|F_c||/\Sigma|F_o|$. [b] $R_w = [\Sigma(|F_o|-|F_c|)^2/\Sigma wF_o^2]^{1/2}$ with $w = 1/[\sigma^2(F_o) + p|F_o|^2]$. [c] From reference [14].

oxygen (O9) atom were refined at this position, each with an s.o.f. of 0.5. Of the four hydrogen atoms with tetrahedral geometry around this position, two have an s.o.f. of 1 (H3a, H3b) and the other two have an s.o.f. of 0.5 (H3c, H3d). The four hydrogen atoms contribute to the ammonium cation, and only H3a and H3b contribute to the water molecule. Another water oxygen atom O8 (s.o.f. = 0.5) was located and refined at an inversion center, linked to two hydrogen atoms also with an s.o.f. of 0.5. Hence, this water molecule is disordered over two positions forming a square plane. Crystal data for **7** were collected at 170 K, making the resolution of the disorder easier than in previously reported structures[12,19,20] for which the crystal data were collected at room temperature.

CCDC-253073 (**2**), CCDC-253074 (**3**), CCDC-253075 (**4**), CCDC-253076 (**5**), CCDC-253077 (**7**), and CCDC-253078 (**8**) contain the supplementary crystallographic data for this paper. These data can be obtained free of charge from The Cambridge Crystallographic Data Centre via www.ccdc.cam.ac.uk/data_request/cif.

ESI-MS method: The ESI-MS experiments were performed on an LCQ ion-trap mass spectrometer (Finnigan-Thermoquest, San Jose, CA, USA) equipped with an electrospray source. Electrospray full-scan spectra, in the range m/z 50–2000, were obtained by infusion through fused silica tubing at 2–10 $\mu L\,min^{-1}$. The LCQ was calibrated (m/z 50–2000) according to the standard calibration procedure of the manufacturer (mixture of caffeine, MRFA, and Ultramark 1621). The temperature of the heated capillary of the LCQ was set at 100 °C, the ion spray voltage was in the range 1–6 kV, and the injection time was 5–200 ms. The solutions were analyzed in the negative mode. Experimental peak values throughout this contribution relate to the m/z ratio of the most abundant peak in the parent group. The calculated m/z values tabulated are those based on the most abundant isotopes. Peak intensities are quoted as percentages of the intensity of the major peak. When citric acid was present in excess in a given solution, its peak (H_3cit^-; m/z 191) was the major feature, and so spectra were acquired in the range m/z 200–1300 and are shown in the range m/z 200–1000 for clarity. As a result of protonation occurring during the ionization process in the spectrometer, species could be detected with a different degree of protonation. Mass spectrometry allows the Fe^{III}:citrate stoichiometry of the complexes to be established. The nuclearity of the complexes is in accord with the results of isotopic pattern calculations.

Three solutions, in which different compounds crystallized, were filtered prior to analysis. The pH of the final solution from which four compounds were successively crystallized (the salt Hneo·NO_3, a nonanuclear species, and compounds **5** and **6**) was 1.5. The pH of the final solution containing only compound **4** was 3.3. The pH of the final solution from which compounds **7** and **8** crystallized was 6.

A series of solutions was prepared with different Fe:cit ratios ranging from 1:1 to 1:20, over the pH range 2.4–9.5, by combining a 0.1 M Fe$(ClO_4)_3\cdot 9H_2O$ solution with 0.2, 0.4, 1 or 2 $mol\,dm^{-3}$ citric acid solutions. The final Fe^{III} concentration in all sample solutions was fixed at $10^{-3}\,mol\,dm^{-3}$. The pH was adjusted with aqueous ammonia. Sample solutions were prepared 20 h prior to analysis and were kept in the dark to avoid photoreduction of Fe^{III}. The spectra did not vary with time, showing that the mixtures had already reached equilibrium when the experiments were carried out. Solutions of which the pH was adjusted with pyridine were also analyzed, and were found to give similar spectra to those obtained with aqueous ammonia solution.

Kinetics of iron exchange from citrate: The kinetics of iron(III) exchange between Fe^{III} citrate complexes and O-TRENSOX or TRENCAMS (the chemical formulae are given in the Supporting Information) was studied in 50 mM aqueous MOPS buffer, pH 7.4, $I = 0.1\,mol\,dm^{-3}$ (NaCl), at $T = 25.0 \pm 0.1$ °C. Fe citrate solutions were prepared by adding an aliquot of a stock solution of $Fe(ClO_4)_3$ (0.01 M in 0.1 M $HClO_4$ standardized by spectrophotometry[21]) to a solution of citric acid to adjust the Fe:cit ratio and then to a buffered solution at pH 7.4 (0.05 M MOPS, 0.1 M NaCl). The Fe^{III} concentration was fixed at $2.0\times10^{-5}\,mol\,dm^{-3}$. Stock solutions of O-TRENSOX and TRENCAMS were prepared in the buffer solution.

Formation of the iron–ligand complexes Fe-O-TRENSOX and Fe-TRENCAMS under pseudo-first-order conditions with respect to the ligand (at least a tenfold excess with respect to the iron concentration) was monitored at 595 and 490 nm, respectively.[16,17] At these wavelengths, Fe citrate solutions do not absorb to any significant extent. Two sets of measurements of iron removal rates were obtained: 1) the first set was collected by varying the ligand concentration (2.0×10^{-4} – $1.8\times10^{-3}\,mol\,dm^{-3}$) for each of the three values of the Fe:cit ratio, 1:5, 1:20, and 1:80; 2) the second set of measurements was realized by varying the Fe:cit molar ratio from 1:10 to 1:80 with the ligand concentration fixed at 4×10^{-4} M in order to determine the dependence of the rate constants on the citrate concentration.

Fast kinetic measurements were performed with a KINSPEC UV (BIO-LOGIC Company, Claix, France) stopped-flow spectrophotometer equipped with a diode-array detector (J. & M.) and connected to a microcomputer. Slow kinetic measurements were made using a Perkin-Elmer Lambda 2 UV/visible spectrophotometer or a Varian Cary 50. The kinetic data were treated on-line with the commercial BIO-KINE program (BIO-LOGIC Company, Claix, France). In each run, equal volumes of solutions of the Fe citrate and the ligand were rapidly mixed. Visible spectra from 400 to 800 nm were recorded at intervals and showed no evidence of intermediate species. The final absorbance indicated that in all cases the formation of the complex with O-TRENSOX or TRENCAMS had reached completion.

Results and Discussion

Crystal structures

Compounds 1–5: Compounds **1–5** were obtained as green-yellow parallelepiped crystals belonging to the triclinic space group $P\bar{1}$ with one molecule of the general formula $(Hbase)_2[Fe_2(cit)_2(H_2O)_2]\cdot n\,H_2O$ in the unit cell. The dianionic dinuclear complexes are centrosymmetric and possess the same structural characteristics. The labeling scheme is shown in Figure 1. Each Fe^{III} ion is in a slightly distorted octahedral $[O_6]$ environment, made up of two fully deprotonated citrate ligands (cit^{4-}) and one aqua ligand. The Fe–O bond lengths are in the range 1.960(2)–2.042(2) Å. Each citrate ligand is tetradentate, bridging the two iron centers through the alkoxo groups (O3 and O3′). The central O6 and one terminal O1 carboxylate are coordinated to the iron atom in a monodentate fashion. The other terminal O4

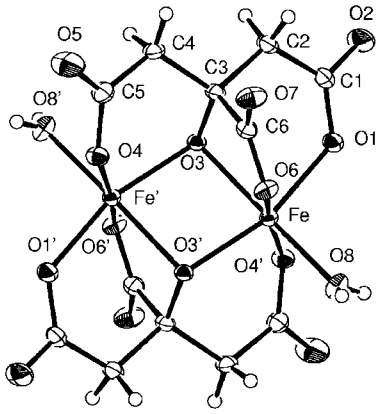

Figure 1. ORTEP representation showing the labeling scheme of the $[Fe_2(cit)_2(H_2O)_2]^{2-}$ ion in compound **2**. The same anion is present in compounds **1–5** (from ref. [14] and this work).

carboxylate is coordinated to the second iron. The Fe, O3, O3′, and Fe′ atoms are in the same plane. The intermetallic distances range from 3.108(1) Å to 3.126(1) Å; the shortest corresponds to the smaller bond angle Fe-O3-Fe′ (100.8(1)°) and is observed in compound **2** (with the imidazolium counter-cation), which has the higher density (ρ_{calcd} = 1.764 g cm^{-3}). The aqua ligands and the non-coordinated oxygen atoms of the citrate ligands in the complex form a three-dimensional hydrogen-bonding network with water molecules and the protonated nitrogen cations.

Compounds **4** and **5** ($(Hneo)_2[Fe_2(cit)_2(H_2O)_2]\cdot 8H_2O$) are polymorphs with a unit cell volume difference of 32 Å^3. The difference appears in the crystal packing of the neocuproinium cations ($Hneo^+$), which in both cases are stacked with alternating orientation (the molecules are related by an inversion center) along the *a* axis. As shown in Figure 2, the stacking mode in compound **5** leads to intermolecular overlap of the aromatic rings, where the nitrogen atoms lie above the center of the next aromatic ring, leading to a short interplanar distance of 3.37 Å, while in compound **4** the aromatic rings are shifted slightly forwards leading to a longer interplanar distance of 3.57 Å. For compounds **1**–**3**, no stacking of the nitrogen heterocycle bases is observed.

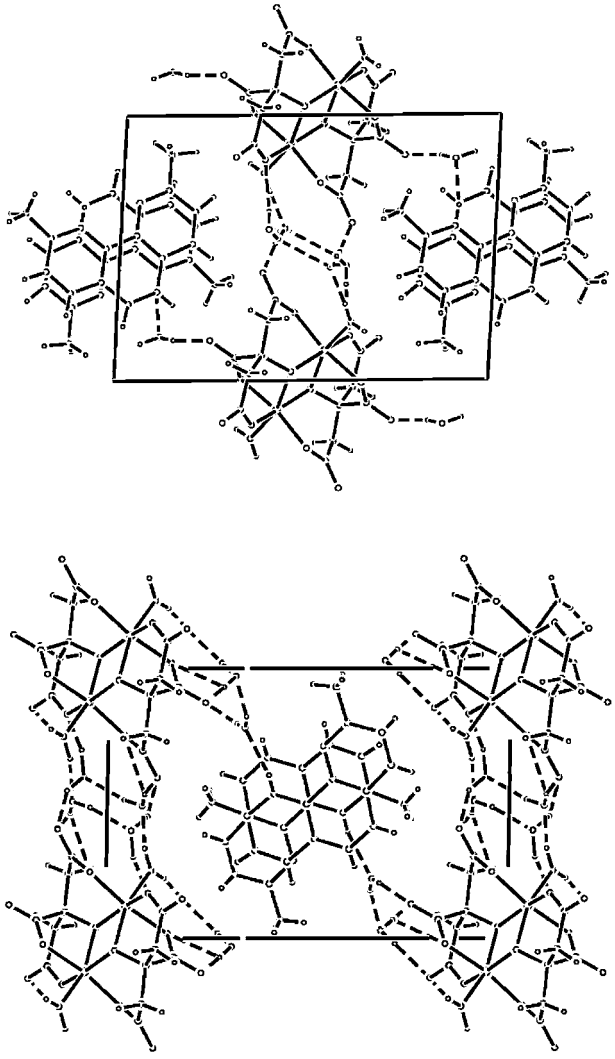

Figure 2. Unit cell representation of $(Hneo)_2[Fe_2(cit)_2(H_2O)_2]\cdot 8H_2O$ in compounds **4** (top) and **5** (bottom). The difference appears in the crystal packing of the neocuproinium cations ($Hneo^+$). Hydrogen bonds are represented by dotted lines.

$(Hneo)_3[Fe_2(Hcit)_3]\cdot 8H_2O$ (6): The crystal structure of **6** reveals a dinuclear trianionic complex as shown in Figure 3, in which the two ferric ions are linked by three triionized citrate ligands, leading to a short intermetallic distance of

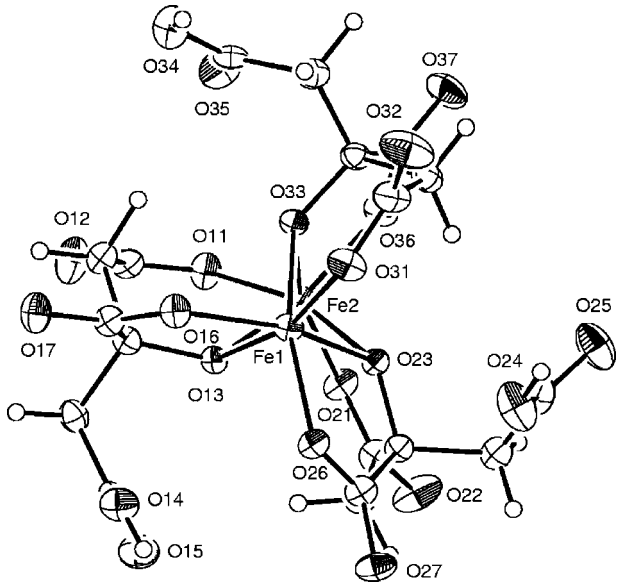

Figure 3. ORTEP representation of the $[Fe_2(Hcit)_3]^{3-}$ ion in compound **6** (from ref. [14] and this work).

2.822(7) Å. Each citrate ligand is tridentate, bridging the two iron centers through the alkoxo group (O13, O23, and O33). The central (O16, O26, and O36) and one terminal (O11, O21, and O31) carboxylate are coordinated in a monodentate fashion to one or other of the iron atoms with the formation of a five- and a six-membered coordination ring, respectively. The other terminal carboxylic group is non-coordinating. In the crystal packing, the planar neocuproinium cations ($Hneo^+$) are stacked with a mean interplane distance of 3.37 Å, leading to an infinite column.

$(NH_4)_5[Fe(cit)_2]\cdot 2H_2O$ (7): The crystal structure of **7** reveals a centrosymmetric pentaanionic complex as shown in Figure 4. The octahedral environment of the iron center is made up of two fully deprotonated tridentate citrate ligands. The citrate is coordinated to the ferric ion in *fac* mode, through the alkoxide O3, the central O6, and one terminal O1 carboxylate in a monodentate fashion. The Fe–O bond lengths are in the range 1.943(1)–2.055(1) Å, and are thus slightly shorter than those given in reference [12] (1.953(2)–2.068(2) Å) (our crystal data were collected at 170 K). The remaining deprotonated terminal carboxylate is non-coordinating, with two close C–O bond lengths (C5–O4 1.243(2),

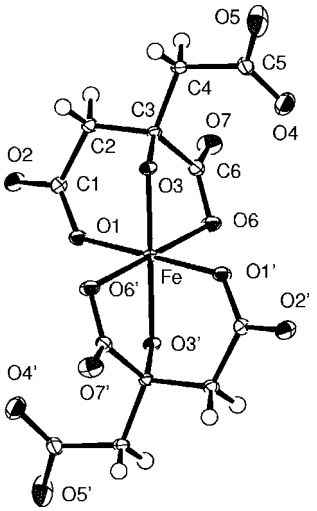

Figure 4. ORTEP representation of the $[Fe(cit)_2]^{5-}$ ion in compound **7**.

C5–O5 1.268(2) Å). The anionic complex is connected to the ammonium cations and water molecules through a network of hydrogen bonds.

$(NH_4)_4[Fe(Hcit)(cit)]\cdot 3H_2O$ (8): The crystal structure of **8** reveals an octahedral complex with two crystallographically independent citrates. The coordination mode of the citrate ligand is similar to that observed in compound **7**. An ORTEP representation is provided in the Supporting Information. The Fe–O bond lengths are in the range 1.932(1)–2.064(1) Å. The *trans* O-Fe-O angles are close to 180°, being in the range 176.34(5)–178.30(6)°. The main difference concerns the non-coordinating carboxylic groups, which are not equivalent in **8**. Considering the difference in the C–O bond lengths (C15–O14 1.207(3), C15–O15 1.312(2), and O15–H15o 0.83 Å), it is clearly evident that one remains protonated while the other is deprotonated with the delocalization of its anionic charge leading to equivalent C–O bond lengths (C25–O24 1.242(2), C25–O25 1.249(3) Å). A very extensive network of hydrogen bonds involves citrate oxygens, water molecules, and ammonium cations.

This compound is isostructural with $(NH_4)_4[Al(Hcit)(cit)]\cdot 3H_2O$ and $(NH_4)_4[Ga(Hcit)(cit)]\cdot 3H_2O$, previously characterized by Matzapetakis et al.[19] In reference [19b], the authors show the formula to be $(NH_4)_4[Ga(Hcit)(cit)]\cdot 3H_2O$ as opposed to the previously suggested $(NH_4)_3[Ga(Hcit)_2]\cdot 4H_2O$.[22] In this latter case, electron density peaks were attributed to water oxygen atoms instead of ammonium nitrogen atoms. This type of error has been highlighted in the Experimental Section in relation to the crystal structure determination of compound **7**. Consequently, both pendant carboxylates are protonated to balance the charge. Moreover, it should be noted that, as for compound **8**, the two non-coordinated carboxylic groups are not equivalent: one remains protonated (C12–O13 1.202(3), C12–O14 1.313(3) Å), while the other is deprotonated (C6–O9 1.261(3), C6–O10 1.231(3) Å).

Some features concerning the coordination of the alkoxy group in the Fe citrate complexes merit further comment. Its coordination (in monodentate mode or in μ_2- or μ_3-alkoxo bridging mode) leads to five- and six-membered chelate rings, which increases the stability of the complexes. In complexes **6** and **8**, the citrate ligand has a non-coordinating carboxylic group (non-deprotonated), whereas the alcohol function is deprotonated. This deprotonation is promoted by Fe^{III}, which is a hard Lewis acid, whereas with Fe^{II},[23] Mn^{II},[20] and Co^{II}[24] the alcohol function remains protonated and hence only coordinates in monodentate mode.

Syntheses of the complexes: Although the various parameters of the synthesis (iron salt, base, pH, Fe:cit ratio, temperature, solvent) are not independent, we tried to delineate their respective influences to establish experimental protocols that would lead to a given complex in a controlled manner.

Influence of the iron salt used: The dinuclear species $[Fe_2(cit)_2(H_2O)_2]^{2-}$ was obtained by using different ferric salts (chloride, perchlorate, and nitrate) as described in the Experimental Section. For example, $(Hpy)_2[Fe_2(cit)_2(H_2O)_2]\cdot 2H_2O$, previously obtained using ferric nitrate,[14] was also isolated when using the chloride or perchlorate salts in this work. Therefore, any role of nitrate ion in the crystallization process of the compounds, which remained unclear in the previous report,[15] may be discounted. From this work, the nature of the counter anion of the ferric salt does not seem to play a role in the synthesis.

Influence of the base: Nitrogen heterocycle bases such as pyridine, imidazole, picoline, or neocuproine, as well as aqueous ammonia, contribute to the deprotonation of the citric acid ligand. Their conjugate cations, $(Hbase)^+$, provide the balance of charge in the solid compounds, promoting the crystal packing by the formation of hydrogen-bonding networks. Bino et al.[15] have already suggested that: "both diiron $[Fe_2(cit)_2(H_2O)_2]^{2-}$ and nonairon complexes exist in equilibrium in aqueous solution and the two different compounds selectively crystallize depending upon which counterion is used to produce solid material" (i.e., pyridine and neocuproine for diiron and nonairon complexes, respectively). The characterization of $(Hneo)_2[Fe_2(cit)_2(H_2O)_2]\cdot 8H_2O$ obtained under different experimental conditions shows that the counterion that leads to the crystallization of the nonanuclear complex also allows the crystallization of the dinuclear species. For compounds **1**–**5**, the different bases play the same role in the synthetic pathway, despite the fact that they induce differences in the crystal packing (vide supra). Nevertheless, compound **6** $(Hneo)_3[Fe_2(Hcit)_3]\cdot 8H_2O$ and the nonanuclear complex $(Hneo)_7[Fe_9O(cit)_8(H_2O)_3]\cdot neo\cdot 61H_2O$[15] are only obtained when neocuproine is used as base. In the crystal structures of these two compounds, as well as in those of compounds **4** and **5**, $(Hneo)_2[Fe_2(cit)_2(H_2O)_2]\cdot 8H_2O$, the planar neocuproine units are stacked in a distinct mode in infinite chains, whereas no

stacking of pyridinium, imidazolium, or picolinium is observed in compounds **1**, **2**, and **3**. The continuous stacking capacity and steric hindrance of neocuproine promotes and stabilizes the crystal lattices of the complexes with this base. Furthermore, the aqueous solution from which the mononuclear species **7** and **8** crystallized contained both pyridinium and ammonium cations. The crystal lattices involved only the ammonium cations in an extensive network of hydrogen bonds. Compounds isostructural to **8**, $(cat)_4[M(Hcit)(cit)]\cdot n\,H_2O$, have been characterized with M = Ga^{3+} or Al^{3+}; cat = NH_4^+, $n = 3$ or cat = K^+, $n = 4$ and show that mononuclear species crystallize with small cations giving a dense material (with ρ_{exp} in a range 1.61–2.05 $g\,cm^{-3}$).[19] The role of the base is thus important in determining which of the solid compounds is produced, and the nature of the counter cation in terms of its steric hindrance determines the crystal packing through the formation of a hydrogen-bonded network and eventually through stacking, filling up the free space in the structure. As we will see later, anionic complexes may be present in the solution, but do not crystallize.

Influence of pH: The species that crystallized in different pH ranges and with different Fe:cit ratios are summarized in Table 3. Three Fe^{III} citrate complexes were crystallized only in acid media. The dinuclear species $[Fe_2(Hcit)_3]^{3-}$, only obtained with neocuproine, was crystallized in the pH range 1.5–2.0. The nonanuclear complex $(Hneo)_7[Fe_9O(cit)_8(H_2O)_3]\cdot neo\cdot 61\,H_2O$ was crystallized at pH 2.3.[15] The dinuclear species $[Fe_2(cit)_2(H_2O)_2]^{2-}$ was crystallized with different counterions (the protonated bases) in the pH range 2.2–3.5. At higher pH, it failed to crystallize. The mononuclear species was isolated as $[Fe(Hcit)(cit)]^{4-}$ at pH 6. The first protonation of the unbound carboxylate occurred at a pH close to the highest pK_a value (6.4) of the carboxylic group of citric acid. The mononuclear dicitrate complex $(NH_4)_5[Fe(cit)_2]\cdot 2\,H_2O$ was obtained in neutral (this work) and basic media (pH 8).[12] The interconversion of species has been investigated for the gallium and aluminum complexes.[19] $[M(Hcit)(cit)]^{4-}$ species (with M = Al^{3+} or Ga^{3+}) have been isolated at pH 4.5–6 and $[M(cit)_2]^{5-}$ at pH 8. We have recently characterized $[Ga(Hcit)(H_2cit)]^{2-}$ species at pH 1.5.[25] It seems that $[M(H_xcit)(H_ycit)]^{(5-x-y)-}$ species (with M = Fe^{3+}, Al^{3+}, or Ga^{3+}) can be observed over a wide pH range, differing only in their protonation state.

Table 3. Crystalline species obtained at different Fe:cit ratios and at different pH.

Fe:cit	$1.5 \le pH \le 2.0$	$2.2 \le pH \le 3.5$	pH 6	$7 \le pH \le 8$
3:1		$[Fe_2(cit)_2(H_2O)_2]^{2-}$		
1:1	$[Fe_2(Hcit)_3]^{3-}$	$[Fe_2(cit)_2(H_2O)_2]^{2-}$		
		$[Fe_9O(cit)_8(H_2O)_3]^{7-}$		
1:2		$[Fe_2(cit)_2(H_2O)_2]^{2-}$		$[Fe(cit)_2]^{5-}$
1:4	$[Fe_2(Hcit)_3]^{3-}$	$[Fe_2(cit)_2(H_2O)_2]^{2-}$	$[Fe(Hcit)(cit)]^{4-}$	$[Fe(cit)_2]^{5-}$

Influence of the Fe:cit ratio and temperature: In aqueous solution, the dinuclear species **2** was obtained with $Fe(ClO_4)_3\cdot 9\,H_2O/H_4cit/im$ in molar ratios of 1:1:4 and 1:2:6. A red powder precipitated when the iron salt was used in excess, while a translucent yellow-green gel was obtained when citric acid was used in excess. Using pyridine, only the dinuclear species **1** $(Hpy)_2[Fe_2(cit)_2(H_2O)_2]\cdot 2\,H_2O$ was obtained when the Fe/H_4cit ratio was varied from 3:1 to 1:4 within the pH range 2.2–3.5. Using a greater excess of citric acid, only the translucent yellow-green gel was obtained, in which colorless crystals of a salt appeared after a few months. The mononuclear species was crystallized with an Fe:cit ratio of 1:2 and was favored at higher citric acid concentrations. An interesting result was obtained using neocuproine. If the solution containing Fe/H_4cit/neocuproine in a molar ratio of 1:1:4 was not heated, only compound **4**, $(Hneo)_2[Fe_2(cit)_2(H_2O)_2]\cdot 8\,H_2O$, crystallized. If the same solution was heated at 60 °C for 30 min and then cooled to room temperature, four different compounds crystallized successively (vide supra). Increasing temperature evidently favors the formation of polynuclear species such as $[Fe_9O(cit)_8(H_2O)_3]^{7-}$. With an excess of citric acid (Fe/H_4cit/neo in a molar ratio of 1:4:3; pH 1.8), the heated solution yields only $(Hneo)_3[Fe_2(Hcit)_3]\cdot 14\,H_2O$.

Influence of solvent: The octanuclear species $(Him)_9[Fe_8(\mu_3\text{-}O)_2(\mu_2\text{-}OH)_2(cit)_6(CH_3CO_2)_2(im)_2]\cdot(ClO_4)\cdot 13\,H_2O$ was obtained only in DMF solution with imidazole as base.[26] Fast evaporation of the solvent from concentrated solutions leads to the dinuclear species identified as $(Him)_2[Fe_2(cit)_2(H_2O)_2]\cdot H_2O\cdot DMF$, while more dilute solutions and slow evaporation favor the octanuclear species. In DMF solution with pyridine, only compound **1**, $(Hpy)_2[Fe_2(cit)_2(H_2O)_2]\cdot 2\,H_2O$, crystallized.

In summary, the Fe:cit ratio and pH are the decisive factors that determine the crystallization of a given complex. Polynuclear complexes crystallize at acid pH and with Fe:cit ratios ranging from 1:1 to 1:4, while mononuclear complexes crystallize at neutral and basic pH with Fe:cit ratios ranging from 1:2 to 1:4. Furthermore, the counter cation, temperature, concentration, and evaporation rate are also important factors. As an example, the obtainment of polynuclear species necessitates elevated temperature, low concentration, and/or very slow evaporation. The results reveal the complexity of iron-citrate chemistry. Different species seem to be in equilibrium in solution, their respective abundances being tuned by the Fe:cit ratio and pH. The occurrence of other species in solution, not yet characterized in the solid state, is possible. We have tried to address this issue by applying electrospray mass spectrometry.

Mass spectrometry: Iron citrate species observed in the different spectra are summarized in Table 4. Figure 5a depicts the spectrum of the residual solution from which the four species $(Hneo)(NO_3)$, the nonanuclear compound $(Hneo)_7[Fe_9O(cit)_8(H_2O)_3]\cdot neo\cdot 61\,H_2O$, and the dinuclear compounds $(Hneo)_2[Fe_2(cit)_2(H_2O)_2]\cdot 8\,H_2O$ (**5**) and $(Hneo)_3[Fe_2$-

Table 4. Negative-ion ESI-MS of iron-citrate species.

Species	*m/z* (calcd)	*m/z* (exptl)
$[Fe(cit)_2H_3]^{2-}$	217.5	217.5
$[Fe(cit)_2H_4]^{-}$	436	435.9
$[Fe_2(cit)_2]^{2-}$	244	243.9
$[Fe_2(cit)_2H]^{-}$	489	488.7
$[Fe_2(cit)_3H_5]^{-}$	681	680.7
$[Fe_3(cit)_3H]^{2-}$	366.5	366.3
$[Fe_3(cit)_3H_2]^{-}$	734	733.6
$[Fe_3O(cit)_3H_3]^{2-}$	375.5	375.2
$[Fe_3O(cit)_3H_4]^{-}$	752	751.4
$[Fe_3(cit)_4H_5]^{2-}$	462.5	462.3
$[Fe_3(cit)_4H_6]^{-}$	926	925.6

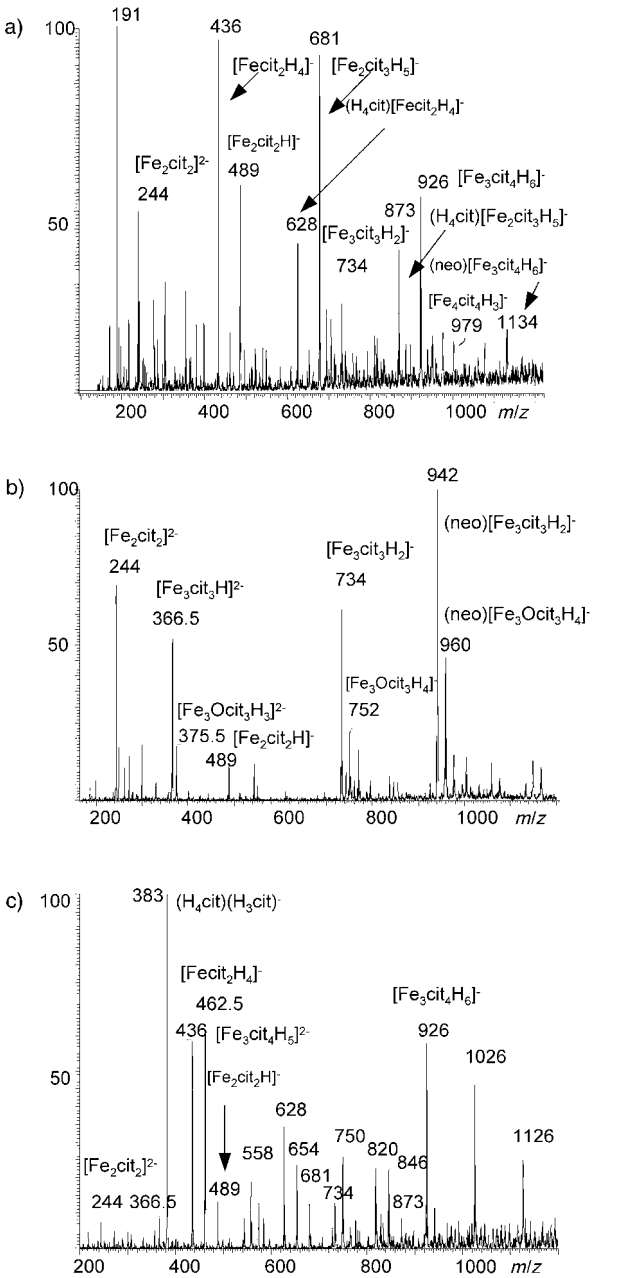

Figure 5. Electrospray mass spectra of residual solutions from which compounds were crystallized : a) $(Hneo)_7[Fe_9O(cit)_8(H_2O)_3]\cdot neo\cdot 61\,H_2O$, **5**, and **6**; b) **4**; c) **7** and **8**.

$(Hcit)_3]\cdot 8\,H_2O$ (**6**) had crystallized. The peaks at *m/z* 244 and 489 are assigned to the $[Fe_2(cit)_2]^{2-}$ and $[Fe_2(cit)_2H]^{-}$ ions, respectively (protonation occurring during the ionization process in the spectrometer), corresponding to the previously crystallized dinuclear complex $[Fe_2(cit)_2(H_2O)_2]^{2-}$. The peak at *m/z* 681 can be attributed either to $(H_4cit)[Fe_2(cit)_2H]^{-}$ and/or to $[Fe_2(cit)_3H_5]^{-}$ species. On the one hand, free citric acid is observed (*m/z* 191 $(H_3cit)^{-}$), and MS-MS of the peak at *m/z* 681 leads to a loss of a neutral fragment of *m/z* 192 (H_4cit), suggesting that $[Fe_2(cit)_2H]^{-}$ (*m/z* 489) is associated with citric acid. On the other hand, a zoom scan of the peak at *m/z* 681 shows that the complex is stable and points to the $[Fe_2(cit)_3H_5]^{-}$ species corresponding to the other previously crystallized dinuclear complex $[Fe_2(Hcit)_3]^{3-}$. The peak at *m/z* 873 corresponds to the association $(H_4cit)[Fe_2(cit)_3H_5]^{-}$. The peaks at *m/z* 436 and 628 are assigned to the mononuclear dicitrate species $[Fe(cit)_2H_4]^{-}$ and $(H_4cit)[Fe(cit)_2H_4]^{-}$, respectively, despite the fact that this did not crystallize from the solution. The peaks at *m/z* 734, 926, 979, and 1134 are assigned to the polynuclear species $[Fe_3(cit)_3H_2]^{-}$, $[Fe_3(cit)_4H_6]^{-}$, $[Fe_4(cit)_4H_3]^{-}$, and $(neo)[Fe_3(cit)_4H_6]^{-}$, respectively. These polynuclear species may correspond to molecular fragments of the nonanuclear complex or to its precursor building blocks present in the solution. The fact that the nonanuclear complex $[Fe_9O(cit)_8(H_2O)_3]^{7-}$ is built up around a central $\{Fe_3O\}$ unit linked in a bridging fashion to six carboxylate moieties arising from two terminal $\{Fe_3(cit)_4\}$ units is in accordance with this hypothesis. No peak is observed at *m/z* values corresponding to the nonanuclear complex $[Fe_9(cit)_8H_x]^{(7-x)-}$ or $[Fe_9O(cit)_8H_x]^{(9-x)-}$.

The spectrum of the residual solution from which only α-$(Hneo)_2[Fe_2(cit)_2(H_2O)_2]\cdot 8\,H_2O$ (**4**) crystallized is depicted in Figure 5b. It reveals the presence of the dinuclear complex, with peaks at *m/z* 244 and 489 corresponding to $[Fe_2(cit)_2]^{2-}$ and $[Fe_2(cit)_2H]^{-}$, respectively. Moreover, the peak at *m/z* 681 is not observed. The pairs of peaks (366.5; 375.5), (734; 752), and (942; 960) are assigned to trinuclear species with a difference in *m/z* of 9 or 18 (H_2O) for the dianions and monoanions, respectively, corresponding to a labile ligand such as aquo OH_2, hydroxo OH^{-}, or oxo O^{2-} (*m/z* 366.5 $[Fe_3(cit)_3H]^{2-}$, *m/z* 375.5 $[Fe_3O(cit)_3H_3]^{2-}$, *m/z* 734 $[Fe_3(cit)_3H_2]^{-}$, *m/z* 752 $[Fe_3O(cit)_3H_4]^{-}$, *m/z* 942 $(neo)[Fe_3(cit)_3H_2]^{-}$, and *m/z* 960 $(neo)[Fe_3O(cit)_3H_4]^{-}$). By analogy with the trinuclear subunits observed in the nonanuclear complex, we suggest in Figure 6 a possible formula for the $[Fe_3(cit)_3H_2]^{-}$ species.

Some trinuclear species have already been identified for aluminum and gallium complexes by NMR spectroscopy and mass spectrometric studies.[19,27,28] Only two trinuclear aluminum complexes, $(NH_4)_5[Al_3(cit)_3(OH)(H_2O)](NO_3)\cdot 6\,H_2O$ and $[Al_3(H_2O)_6][Al_3(cit)_2(OH)_2(H_2O)_4]_2$-

The spectrum of the residual solution from which $(NH_4)_5[Fe(cit)_2]\cdot 2\,H_2O$ (**7**) and $(NH_4)_4[Fe(Hcit)(cit)]\cdot 3\,H_2O$ (**8**) crystallized is depicted in Figure 5c. It reveals the presence of free citric acid (*m/z* 383 $(H_4cit)(H_3cit)^{-}$) and mononuclear,

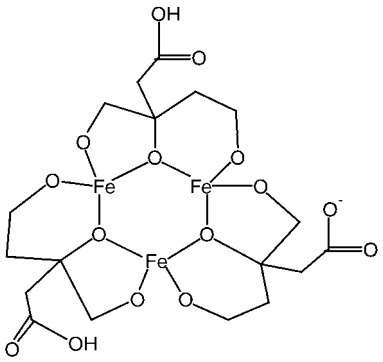

Figure 6. Proposed formula for the trinuclear $[Fe_3(cit)_3H_2]^-$ species observed in ESI-MS. In solution, the coordination sphere of the iron is completed with H_2O ligands.

dinuclear, and trinuclear species. The peaks at *m*/*z* 217.5, 436, 628, and 820 can be assigned to the mononuclear dicitrate species $[Fe(cit)_2H_3]^{2-}$, $[Fe(cit)_2H_4]^-$ and the anion associated with citric acid $(H_4cit)[Fe(cit)_2H_4]^-$ and $(H_4cit)_2$-$[Fe(cit)_2H_4]^-$, respectively. The peaks at *m*/*z* 244, 489, 681, and 873 can be assigned to the dinuclear dicitrate $[Fe_2$-$(cit)_2]^{2-}$, $[Fe_2(cit)_2H]^-$, $(H_4cit)[Fe_2(cit)_2H]^-$, and $(H_4cit)_2[Fe_2$-$(cit)_2H]^-$, respectively. The trinuclear species is observed either as the dianion $[Fe_3(cit)_4H_5]^{2-}$ at *m*/*z* 462, and associated with free citric acid at *m*/*z* 558, 654, 750, and 846 $(H_4cit)_n$-$[Fe_3(cit)_4H_5]^{2-}$ (with $n = 1$–4), or as the monoanion at *m*/*z* 926 $[Fe_3(cit)_4H_6]^-$ and associated with perchloric acid at *m*/*z* 1026 and 1126 $(HClO_4)_n[Fe_3(cit)_4H_6]^-$ (with $n = 1, 2$). Small peaks at *m*/*z* 366.5 and 734 are assigned to the trinuclear $[Fe_3(cit)_3H]^{2-}$ and $[Fe_3(cit)_3H_2]^-$ species, respectively.

This ESI-MS study of solutions from which crystals had been obtained revealed the existence of trinuclear species that did not crystallize, in addition to the crystallized species. Moreover, this study provided evidence for the occurrence of species in equilibrium with different Fe:cit stoichiometries (1:2, 2:2, 2:3, 3:3, and 3:4).

Table 5 summarizes the principal features of ESI mass spectra recorded as a function of pH with Fe:cit ratios in the range from 1:1 to 1:20. It shows the relative evolution of the peak intensities of the identified species (1:2, 2:2, 2:3, 3:3, and 3:4). In acid media, species are often associated with perchloric acid derived from the iron salt. When the concentration of citrate is increased, species become associated with free citric acid. The strong peak intensity of the $[Fe_2(cit)_2H_{1+x}]^{(1-x)-}$ species (observed at Fe:cit ratios of 1:1 to 1:2 at acid pH) decreases with increasing *n* in the Fe:cit 1:*n* ratio. This species is present at any pH. The trinuclear $[Fe_3(cit)_3H_{2+x}]^{(1-x)-}$ or $[Fe_3(cit)_4H_{6+x}]^{(1-x)-}$ species give rise to strong peaks at Fe:cit ratios of 1:2 to 1:4. These species failed to crystallize (except in the form of the nonanuclear complex, which allows coordination of the pendant carboxylate groups), despite the fact that they occur over the entire pH range. For an Fe:cit ratio of 1:10 (Figure 7), the peak intensity of the trinuclear species decreases at acidic and basic pH, while it is still strong at neutral pH. At an Fe:cit ratio of 1:20, trinuclear species are observed only at neutral pH.

The $[Fe(cit)_2H_{4-x}]^{(1+x)-}$ species is clearly observed for an Fe:cit ratio of 1:2 at pH 9, corresponding to the experimental conditions used by Matzapetakis et al.[12] for the crystallization of the $[Fe(cit)_2]^{5-}$ species. For a given Fe:cit ratio, the

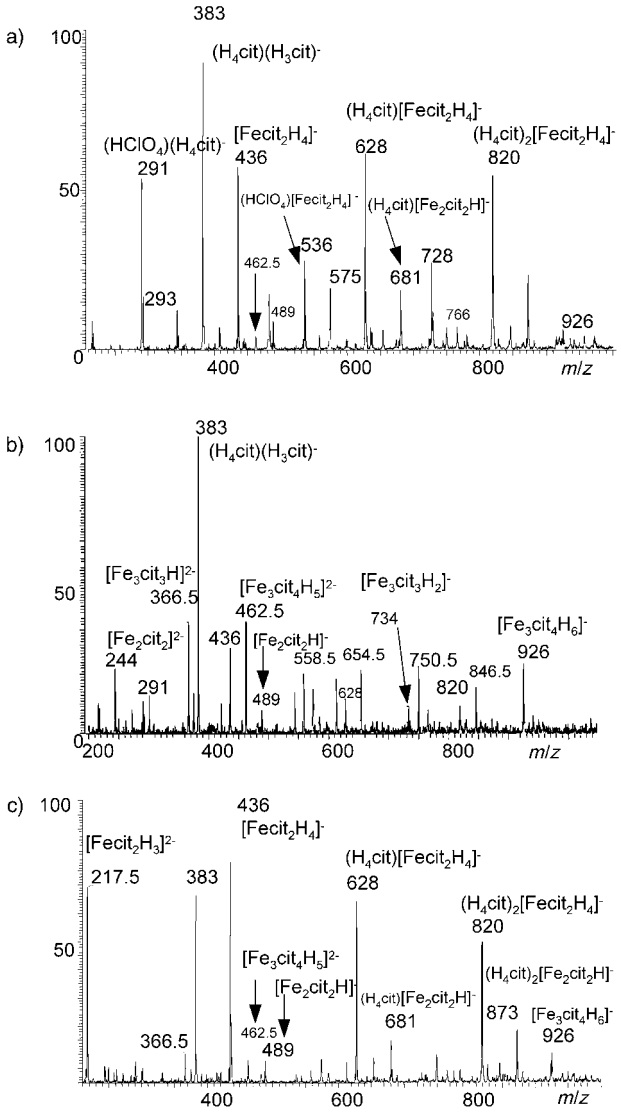

Figure 7. Electrospray mass spectra of solutions with Fe:cit ratio 1:10 at different pH. a) pH 2.4; b) pH 6.5; c) pH 9.5.

peak intensity of the $[Fe(cit)_2H_{4-x}]^{(1+x)-}$ species increases with increasing pH. For an Fe:cit ratio of 1:10 (Figure 7), this peak becomes the major one only at acidic and basic pH. For an Fe:cit ratio of 1:20, the mononuclear complex is the major species at any pH.

The species observed by ESI-MS are in accordance with the results of the crystal growth studies. Polynuclear complexes are predominant at low Fe:cit ratios (1:1 to 1:4). The mononuclear dicitrate becomes predominant at basic pH with an Fe:cit ratio of 1:4. Its concentration increases with increasing *n* in the Fe:cit 1:*n* ratio. At neutral pH, polynu-

Table 5. Species observed by ESI-MS as a function of pH and Fe:cit molar ratio.[a]

Fe:cit ratio	Acid pH species, *m/z*	Neutral pH species, *m/z*	Basic pH species, *m/z*
1:1	**pH 3.5** **$[Fe_2(cit)_2]^{2-}$ 244 vs** $[Fe_2(cit)_2H]^-$ 489 w $(HClO_4)[Fe_2(cit)_2H]^-$ 589 w $[Fe_2(cit)_3H_5]^-$ 681 vw $(HClO_4)[Fe_2(cit)_3H_5]^-$ 781 w $[Fe_3(cit)_3H]^{2-}$ 366.5 vw $[Fe_3(cit)_3H_2]^-$ 734 m $(HClO_4)[Fe_3(cit)_3H_2]^-$ 834 m $[Fe_3(cit)_4H_6]^-$ 926 w		
1:2	**pH 3.5** **$[Fe_2(cit)_2]^{2-}$ 244 vs** $[Fe(cit)_2H_4]^-$ 436 vw $[Fe_2(cit)_2H]^-$ 489 vw $[Fe_3(cit)_3H]^{2-}$ 366.5 m $[Fe_3(cit)_3H_2]^-$ 734 m $(HClO_4)[Fe_3(cit)_3H_2]^-$ 834 vw **$[Fe_3(cit)_4H_6]^-$ 926 vs**	**pH 7.0** $[Fe_2(cit)_2]^{2-}$ 244 vw $[Fe_2(cit)_2H]^-$ 489 vw **$[Fe_3(cit)_3H]^{2-}$ 366.5 vs** $[Fe_3(cit)_3H_2]^-$ 734 m $(HClO_4)[Fe_3(cit)_3H_2]^-$ 834 w $[Fe_3O(cit)_3H_3]^{2-}$ 375.5 w $[Fe_3O(cit)_3H_4]^-$ 752 w	**pH 9.0** $[Fe(cit)_2H_4]^-$ 436 m $[Fe_2(cit)_2]^{2-}$ 244 m $[Fe_2(cit)_2H]^-$ 489 w **$[Fe_3(cit)_3H]^{2-}$ 366.5 vs** $[Fe_3(cit)_3H_2]^-$ 734 s $[Fe_3(cit)_4H_5]^{2-}$ 462.5 w **$[Fe_3(cit)_4H_6]^-$ 926 vs**
1:4	**pH 3.5** $[Fe(cit)_2H_4]^-$ 436 w $[Fe_2(cit)_2]^{2-}$ 244 m $[Fe_2(cit)_2H]^-$ 489 w $[Fe_2(cit)_3H_5]^-$ 681 vw $(HClO_4)[Fe_2(cit)_3H_5]^-$ 781 w $[Fe_3(cit)_3H]^{2-}$ 366.5 s $[Fe_3(cit)_3H_2]^-$ 734 m $(HClO_4)[Fe_3(cit)_3H_2]^-$ 834 w $[Fe_3O(cit)_3H_3]^{2-}$ 375.5 vw $[Fe_3O(cit)_3H_4]^-$ 752 w $[Fe_3(cit)_4H_5]^{2-}$ 462.5 s **$[Fe_3(cit)_4H_6]^-$ 926 vs**	**pH 6.8** $[Fe(cit)_2H_4]^-$ 436 w $[Fe_2(cit)_2]^{2-}$ 244 w $[Fe_2(cit)_2H]^-$ 489 vw **$[Fe_3(cit)_3H]^{2-}$ 366.5 vs** $[Fe_3(cit)_3H_2]^-$ 734 w $(HClO_4)[Fe_3(cit)_3H_2]^-$ 834 w $[Fe_3O(cit)_3H_3]^{2-}$ 375.5 vs $[Fe_3O(cit)_3H_4]^-$ 752 w $[Fe_3(cit)_4H_5]^{2-}$ 462.5 s **$[Fe_3(cit)_4H_6]^-$ 926 vs**	**pH 9.0** $[Fe(cit)_2H_3]^{2-}$ 217.5 s **$[Fe(cit)_2H_4]^-$ 436 vs** $(H_4cit)_n[Fe(cit)_2H_4]^-$ 628 m, 820 w $[Fe_2(cit)_2]^{2-}$ 244 w $[Fe_2(cit)_2H]^-$ 489 w $(H_4cit)[Fe_2(cit)_2H]^-$ 681 w $[Fe_3(cit)_3H]^{2-}$ 366.5 m $[Fe_3(cit)_3H]^{2-}$ 734 w $[Fe_3O(cit)_3H_3]^{2-}$ 375.5 m $[Fe_3O(cit)_3H_4]^-$ 752 w $[Fe_3(cit)_4H_5]^{2-}$ 462.5 m $[Fe_3(cit)_4H_6]^-$ 926 s
1:10	**pH 2.4** **$[Fe(cit)_2H_4]^-$ 436 vs** **$(H_4cit)_n[Fe(cit)_2H_4]^-$ 628 vs**, 820 vs $[HClO_4][Fe(cit)_2H_4]^-$ 536 m $[HClO_4][Fe_2(cit)_2]^{2-}$ 344 w $[Fe_2(cit)_2H]^-$ 489 vw $(H_4cit)_n[Fe_2(cit)_2H]^-$ 681 w, 873 w $[Fe_3(cit)_4H_5]^{2-}$ 462.5 vw $[Fe_3(cit)_4H_6]^-$ 926 vw	**pH 6.5** **$[Fe(cit)_2H_4]^-$ 436 vs** $(H_4cit)_n[Fe(cit)_2H_4]^-$ 628 m, 820 w $[Fe_2(cit)_2]^{2-}$ 244 s $[Fe_2(cit)_2H]^-$ 489 w **$[Fe_3(cit)_3H]^{2-}$ 366.5 vs**, $(H_4cit)_n[Fe_3(cit)_3H]^{2-}$ 558 m, 654 m, 750 s, 846 m $[Fe_3(cit)_3H_2]^-$ 734 m **$[Fe_3(cit)_4H_5]^{2-}$ 462.5 vs** $[Fe_3(cit)_4H_6]^-$ 926 s	**pH 9.5** $[Fe(cit)_2H_3]^{2-}$ 217.5 s **$[Fe(cit)_2H_4]^-$ 436 vs** $(H_4cit)_n[Fe(cit)_2H_4]^-$ 628 s, 820 m $[Fe_2(cit)_2]^{2-}$ 489 vw $(H_4cit)_n[Fe_2(cit)_2H]^-$ 681 vw, 873 w $[Fe_3(cit)_4H_5]^{2-}$ 462.5 vw $[Fe_3(cit)_4H_6]^-$ 926 vw
1:20	**pH 2.4** $[Fe(cit)_2H_4]^-$ 436 s **$(H_4cit)_n[Fe(cit)_2H_4]^-$ 628 vs, 820 vs** $[Fe_2(cit)_2H]^-$ 489 vw $(H_4cit)_n[Fe_2(cit)_2H]^-$ 681 w, 873 w, 1064 w	**pH 6.8** **$[Fe(cit)_2H_4]^-$ 436 vs** $(H_4cit)_n[Fe(cit)_2H_4]^-$ 628 s, 820 m $[Fe_2(cit)_2H]^-$ 489 vw $(H_4cit)_n[Fe_2(cit)_2H]^-$ 681 vw, 873 vw, 1064 vw $[Fe_3(cit)_3H]^{2-}$ 366.5 m $(H_4cit)_n[Fe_3(cit)_3H]^{2-}$ 558 vw, 654 vw, 750 vw, 846 vw $[Fe_3(cit)_3H_2]^-$ 734 vw $[Fe_3(cit)_4H_5]^{2-}$ 462.5 w $[Fe_3(cit)_4H_6]^-$ 926 w	**pH 9.2** $[Fe(cit)_2H_3]^{2-}$ 217.5 s **$[Fe(cit)_2H_4]^-$ 436 vs** $(H_4cit)_n[Fe(cit)_2H_4]^-$ 628 s, 820 m $[Fe_2(cit)_2]^{2-}$ 489 vw $(H_4cit)_n[Fe_2(cit)_2H]^-$ 681 vw, 873 vw

[a] Species giving rise to major peak intensities are written in bold. Peak intensities are noted as percentages of the major peak intensity observed for an iron citrate species: 100–80 %: vs (very strong); 80–60 %: s (strong); 60–40 %: m (medium); 40–20 %: w (weak); 20–5 %: vw (very weak).

clear species progressively disappear in favor of mononuclear species as the concentration of citrate is increased from an Fe:cit ratio of 1:10.

Kinetics of iron uptake from citrate: Kinetic studies of the transfer of citrate-bound Fe^{III} to the competing ligands O-TRENSOX and TRENCAMS were conducted in water at pH 7.4 (25 °C). As these experimental conditions are close to those used in the ESI-MS studies, it was assumed that the same species would be involved. In all measurement runs, two well-separated first-order absorbance increases were observed (Figure 8), the first on a time scale of several tens of seconds (recorded with a stopped-flow apparatus), and the second on a time scale of several tens of minutes (recorded with a UV/Vis spectrophotometer). In each case, the final absorbance of the reaction solution indicated that the exchange reaction had reached completion. We measured the amplitude of the absorbance jump for each stage with good

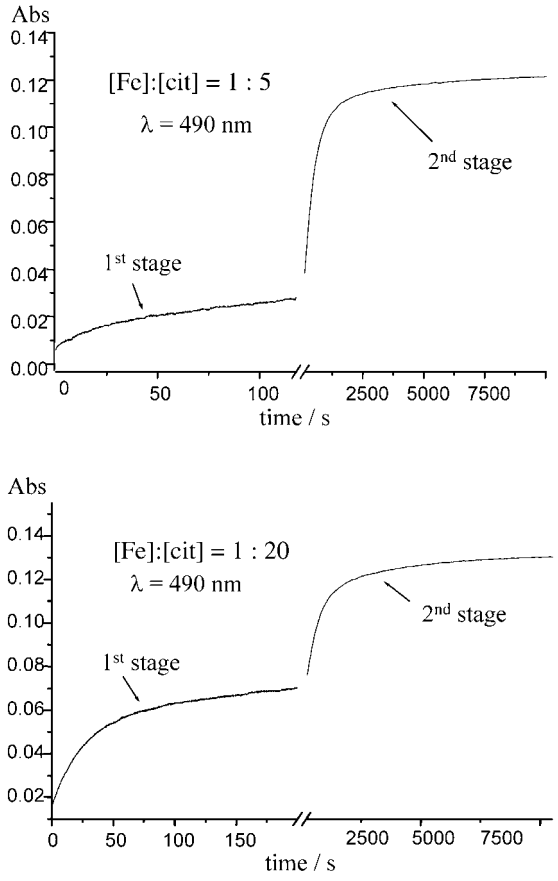

Figure 8. Overall absorbance increases recorded versus time at λ = 490 nm for the transfer of citrate-bound Fe to TRENCAMS. Experimental conditions: $[Fe^{III}]$ = 0.02 mM, [TRENCAMS] = 0.40 mM, pH 7.4 (0.05 M MOPS buffer, 0.1 M NaCl), T = 25 °C.

accuracy. Data were collected from experiments with various concentrations of the ligands O-TRENSOX or TRENCAMS, at three different values of the Fe:cit molar ratio. An interesting feature is that the absorbance jump of each stage was found to be independent of the type of ligand and of its concentration, but significantly dependent on the Fe:cit ratio. We report in Table 6 the mean values of the first absorbance jump expressed as a percentage of the total absorbance. They indicate that the first jump increases as the concentration of citrate increases, while the reverse is observed for the second jump (Figure 8).

Data in the literature demonstrate that $[Fe(cit)_2]^{5-}$ is the major species at high citrate concentrations, while polynuclear species are the major species at low citrate concentrations. The two kinetic stages were found to fit the speciation of the mononuclear $[Fe(cit)_2]^{5-}$ and polynuclear complexes at the equilibrium according to the Fe:cit ratio. The first absorbance jump directly measures the formation of the complex between the incoming ligand (TRENCAMS or O-TRENSOX) and iron removed from $[Fe(cit)_2]^{5-}$. The second stage involves the polynuclear species, which reacts about 20 (for TRENCAMS) to 100 (for O-TRENSOX) times slower than the mononuclear species. Of course, while the mononuclear species can be considered as being well defined, the term "polynuclear species" may represent several complexes with nuclearity of two or more. The molar fractions of the mononuclear and of the polynuclear species can thus be evaluated from the percentages of the absorbances in the first and second jumps, respectively. A calculation can be made based on the mass balance equation and the absorbance data ($[Fe_n(cit)_y]$ denotes the polynuclear complexes, charges being omitted) [Eq. (1)].

Table 6. Amplitude of the first jump and the corresponding molar fractions of $[Fe(cit)_2]$ as a function of the Fe:cit molar ratio for the kinetics of transfer.

$[Fe^{III}]$:[cit][a]	1:5	1:20	1:80
	O-TRENSOX		
amp. [%][b]	25 ± 5	50 ± 5	78 ± 4
$x_2[Fe(cit)_2]$[c]	0.40	0.67	0.88
$x_3[Fe(cit)_2]$[d]	0.50	0.75	0.91
	TRENCAMS		
amp. [%][b]	22 ± 3	50 ± 5	80 ± 5
$x_2[Fe(cit)_2]$[c]	0.36	0.67	0.89
$x_3[Fe(cit)_2]$[d]	0.46	0.75	0.92

[a] $[Fe^{III}]$ = 0.02 mM, [cit]: 0.1–1.6 mM, [Ligand] = 0.4–1.5 mM. [b] amp. [%] refers to the amplitude of the first absorbance jump as a percentage of the total absorbance change. The values are the average of three experiments for each ligand concentration (0.04, 0.06, 0.08, 0.10, and 0.15 mM). [c] Molar fraction of $[Fe(cit)_2]$ calculated if the polynuclear complex is $[Fe_2(cit)_2]$ only. [d] Molar fraction of $[Fe(cit)_2]$ calculated if polynuclear complex is $[Fe_3(cit)_y]$ only.

$$[Fe^{III}]_{tot} = [Fe(cit)_2] + \sum n\,[Fe_n(cit)_y] \quad (1)$$

As $[Fe_2(cit)_2]$ and $[Fe_3(cit)_y]$ are the only polynuclear species that have been characterized by ESI-MS, a simple calculation can be made by considering two limiting cases where n = 2 or 3 in the mass balance equations (2) and (3), respectively.

$$[Fe]_{tot} = [Fe(cit)_2] + 2\,[Fe_2(cit)_2] \quad (2)$$

$$[Fe]_{tot} = [Fe(cit)_2] + 3\,[Fe_3(cit)_y] \quad (3)$$

The values of the molar fraction of $[Fe(cit)_2]$ are reported in Table 6, thus giving its lower and upper limit for a mixture of di- and trinuclear complexes.

Our results clearly show that the amount of the mononuclear species greatly increases (from 40% to 90%) as the concentration of citrate is increased (from an Fe:cit ratio of 1:5 to 1:80), while the reverse is true for the polynuclear species. Nevertheless, a few percent of polynuclear species is still present at high citrate concentration. This is consistent with the ESI-MS data, which show that the distribution of the major species reverses at an Fe:cit ratio of about 1:10. Furthermore, Spiro et al.[8] have shown that in alkaline media the presence of excess citrate suppresses the amount of polynuclear species.

Analysis of the absorbance versus time data gave the pseudo-first-order rate constants k_1^{obs} (fast stage) and k_2^{obs} (slow stage). The two stages could be analyzed independent-

ly since the expected conversion of polynuclear complexes into the mononuclear complex is very slow (requiring several hours).[8] The exchange of iron from each complex is thus assumed to have no effect on the mononuclear-polynuclear balance.

Fast stage: The rate constants k_1^{obs} were found to vary linearly with the concentration of ligand L at a constant Fe:cit ratio and to decrease with increasing n in the Fe:cit 1:n ratio at constant ligand concentration (rate constants are collected in Tables S3 and S4 in the Supporting Information). The kinetic data are interpreted in terms of a two-step process involving a fast pre-equilibrium of the $[Fe(cit)_2]^{5-}$ dissociation followed by coordination of L and removal of citrate (where $m = 4$ for O-TRENSOX and $m = 5$ for TRENCAMS, according to the pK_a values of the hydroxy groups and including the three sulfonate groups) (Scheme 1). At pH 7.4, cit^{4-} is then transformed into $Hcit^{3-}$.

The variation of k_1^{obs} with respect to [L] and [cit] can thus be described by the rate law given in Equation (7):

$$k_1^{obs} = k_1 K[L]/([cit] + K) \quad (7)$$

$$[Fe(cit)_2]^{5-} \rightleftharpoons [Fe(cit)]^{-} + cit^{4-} \quad K \quad (4)$$

$$[Fe(cit)]^{-} + L^{m-} \longrightarrow [Fe(cit)L]^{(m+1)-} \quad k_1 \quad (5)$$

$$\downarrow \text{fast}$$

$$FeL^{(m-3)-} + cit^{4-} \quad (6)$$

Scheme 1.

A nonlinear least-squares fit of k_1^{obs} according to Equation (7) yielded the values:

$k_1 = 232 \pm 12\,M^{-1}s^{-1}$, $K = 0.0090 \pm 0.0048\,M$ for L = O-TRENSOX

$k_1 = 134 \pm 7\,M^{-1}s^{-1}$, $K = 0.00260 \pm 0.00046\,M$ for L = TRENCAMS

The values of K calculated from two independent sets of measurements were in reasonable agreement. Plasmatic non-transferrin-bound iron, including iron from citrate, is a potential target in the treatment of iron overload.[30] As in blood plasma the Fe:cit ratio is close to 1:100, $[Fe(cit)_2]^{5-}$ is the major species. Our results indicate that O-TRENSOX and TRENCAMS are able to rapidly take up this iron. The slight difference in reactivity between O-TRENSOX and TRENCAMS (232 and $134\,M^{-1}s^{-1}$, respectively) could be related to a charge effect (4^- and 5^-, respectively).

Slow stage: The rate constants k_2^{obs} were found to be independent of the Fe:cit ratio. For O-TRENSOX, a linear variation of k_2^{obs} versus the ligand concentration was observed, while for TRENCAMS k_2^{obs} exhibited a saturation behavior versus the ligand concentration (see Tables S5 and S6 in the Supporting Information). A common scheme of a two-step process can be proposed, involving a fast pre-equilibrium of formation of the citrate–Fe–ligand ternary complex followed by its dissociation into FeL and citrate ion (the charges on the complexes are omitted) (Scheme 2).

According to this scheme, the variation of k_2^{obs} with [L] can be described by the rate law given in Equation (10).

$$k_2^{obs} = k_2 K'[L]/(1 + K'[L]) \quad (10)$$

$$[Fe_n cit_y] + L \rightleftharpoons [Fe_n cit_y L] \quad K' \quad (8)$$

$$[Fe_n cit_y L] \longrightarrow FeL + cit^{4-} + [Fe_{n-1} cit_{y-1}] \quad k_2 \quad (9)$$

$$L \downarrow \text{fast}$$

$$(n\text{-}1)\,FeL + (y\text{-}1)\,cit^{4-}$$

Scheme 2.

For TRENCAMS, the nonlinear least-squares fit of k_2^{obs} according to Equation (10) yielded the values of k_2 and K' for each Fe:cit value. For O-TRENSOX, the linear variation of k_2^{obs} *versus* [L] implies that $K'[L] \ll 1$ and so $K' \leq \approx 70\,M^{-1}$ as $[L] \leq 0.0015\,M$ under our experimental conditions. All the values are reported in Table 7.

Consistent values of k_2 and k_2K' are obtained at the three different Fe:cit ratios. It may be inferred that the fast and slow processes occur independently. A similar mechanism has been proposed by Faller and Nick[31] for the removal of iron from citrate by Desferrioxamine B and 3-hydroxy-1,2-dimethyl-4-pyridone at 37 °C with an Fe:cit ratio of 1:5. The overall rate constants obtained here, expressed as k_2K', 2.2 and $7.1\,M^{-1}s^{-1}$ for O-TRENSOX and TRENCAMS, respectively (at 25 °C), are close to that measured with Desferrioxamine ($4\,M^{-1}s^{-1}$ at 37 °C). The efficacy of citrate displacement decreases in the order: catecholate > hydroxamate ≈ 8-hydroxyquinolinate. The kinetics of removal of iron appears to be relatively fast, which suggests that the polynuclear species are di- or trinuclear species rather than species of higher nuclearity. Indeed, recent kinetic studies have shown that high nuclearity ferric complexes react much more slowly owing to larger steric effects compared to those with di- or trinuclear species.[32] It can be emphasized that ESI-MS and kinetic studies provide consistent results.

Table 7. Kinetic constants for the transfer of Fe from citrate to the competing ligand according to Scheme 2.

$[Fe^{III}]$:[cit][a]	1:5	1:20	1:80
	O-TRENSOX		
k_2K' $[M^{-1}s^{-1}]$	2.20 ± 0.36	2.93 ± 0.15	2.11 ± 0.28
	TRENCAMS		
k_2 $[s^{-1}]$	0.0096 ± 0.0019	0.0075 ± 0.0013	0.0079 ± 0.0013
K' $[M^{-1}]$	743 ± 232	925 ± 328	948 ± 322
k_2K' $[M^{-1}s^{-1}]$	7.1	6.9	7.5

[a] $[Fe^{III}] = 0.025\,mM$, [cit]: 0.125–2 mM.

Conclusion

The most notable feature of our study is that several different iron(III) citrate complexes have been crystallized by varying the experimental conditions. To date, six anionic complexes have been structurally characterized in the solid state, by ourselves or others, and we have established the respective experimental conditions leading to each of them. These complexes have been identified in solution (in different protonation states) on the basis of electrospray ionization mass spectrometry studies, except for the nonanuclear species, for which only the precursor building blocks could be detected as trinuclear species in solution. All these results emphasize the complexity of iron(III) citrate chemistry. It is obvious that the expression "ferric citrate", as widely used in the literature (especially in biology), does not describe one clearly defined chemical species, but in most cases several species in equilibrium, the nature of which is essentially tuned by the Fe:cit ratio and pH. Kinetic studies of iron uptake from citrate by iron chelators at pH 7.4 are in agreement with the ESI-MS results and allow calculation of the speciation of the citrate complexes. Furthermore, they emphasize the ability of chelators to withdraw non-transferrin-bound plasma iron, which is a target for iron chelation therapy. Our results are also of relevance to the iron transport system of *E. coli*, in which a so-called ferric citrate system has been characterized.[4,11] Two crystallographic structures of the dinuclear $[Fe_2(cit)_2]^{2-}$ ligated to FecA have been obtained: 1) the first[13a] under conditions (Fe:cit ratio 1:1) for which our results show that the dinuclear species is favored, and 2) the second[13b] under conditions (Fe:cit ratio 1:20) for which ESI-MS and kinetic data provide evidence of the presence of di- and trinuclear species, yet the mononuclear dicitrate remains the predominant species. The mononuclear dicitrate and the dinuclear dicitrate species are both candidates for the species recognized by the bacterial transport system. Better knowledge of the speciation of the citrate complexes in solution may provide additional support to interpret the results of iron nutrition studies of *E. coli* (and some selected mutants) by iron citrate. Further studies are in progress in our laboratory concerning this point.

Acknowledgements

We are grateful to Prof. E. Saint-Aman (Grenoble, France) for fruitful discussions.

[1] J. P. Glusker, *Acc. Chem. Res.* **1980**, *13*, 345–352.
[2] L. O. Tiffin, *Plant Physiol.* **1966**, *41*, 515–518.
[3] A. Pich, G. Scholz, K. Seifert, *J. Plant Physiol.* **1991**, *137*, 323–326.
[4] C. Härle, I. S. Kim, A. M. Angerer, W. Braun, *EMBO J.* **1995**, *14*, 1430–1438.
[5] N. J. Rahway, *The Merck Index* (Ed.: M. Windholz), Merck, **1983**.
[6] P. Baret, C. Beguin, H. Boukhalfa, C. Caris, J.-P. Laulhère, J.-L. Pierre, G. Serratrice, *J. Am. Chem. Soc.* **1995**, *117*, 9760–9761.
[7] J.-L. Pierre, I. Gautier-Luneau, *Biometals* **2000**, *13*, 91–96.
[8] T. G. Spiro, G. Bates, P. Saltman, *J. Am. Chem. Soc.* **1967**, *89*, 5559–5562.
[9] R. B. Martin, *J. Inorg. Biochem.* **1986**, *28*, 181–187.
[10] H. Yokol, T. Mitani, Y. Mori, S. Kawata, *Chem. Lett.* **1994**, 281–284.
[11] V. Braun, K. Hantke, W. Köster, "Iron Transport and Storage in Microorganisms, Plants and Animals" in *Metal Ions in Biological Systems*, *Vol. 35* (Eds.: A. Sigel, H. Sigel), Marcel Dekker, **1998**, pp. 239–327.
[12] M. Matzapetakis, C. P. Raptopoulou, A. Tsohos, V. Papaefthymiou, N. Moon, A. Salifoglou, *J. Am. Chem. Soc.* **1998**, *120*, 13266–13267.
[13] a) A. D. Ferguson, R. Chakraborty, B. S. Smith, L. Esser, D. van-der Helm, J. Deisenhofer, *Science* **2002**, *295*, 1715–1719; b) W. W. Yue, S. Griaot, S. K. Buchanan, *J. Mol. Biol.* **2003**, *332*, 353–368.
[14] I. Shweky, A. I. Bino, D. P. Goldberg, S. J. Lippard, *Inorg. Chem.* **1994**, *33*, 5161–5162.
[15] A. I. Bino, I. Shweky, S. Cohen, E. R. Bauminger, S. J. Lippard, *Inorg. Chem.* **1998**, *37*, 5168–5172.
[16] G. Serratrice, H. Boukhalfa, C. Béguin, P. Baret, C. Caris, J.-L. Pierre, *Inorg. Chem.* **1997**, *36*, 3898–3910.
[17] F. Thomas, C. Béguin, J.-L. Pierre, G. Serratrice, *Inorg. Chim. Acta* **1999**, *291*, 148–157.
[18] TEXSAN, Single-crystal structure analysis software, version 1.7, Molecular Structure Corporation, 3200 Research Forest Drive, The Woodlands, TX 77381, USA, **1995**.
[19] a) M. Matzapetakis, C. P. Raptopoulou, A. Terkis, A. Lakatos, T. Kiss, A. Salifoglou, *Inorg. Chem.* **1999**, *38*, 618–619; b) M. Matzapetakis, M. Kourgiantakis, M. Dakanali, C. P. Raptopoulou, A. Terkis, A. Lakatos, T. Kiss, I. Banyai, L. Iordanidis, T. Mavromoutakos, A. Salifoglou, *Inorg. Chem.* **2001**, *40*, 1734–1744.
[20] M. Matzapetakis, N. Karligiano, A. Bino, M. Dakanali, C. P. Raptopoulou, V. Tangoulis, A. Terkis, J. Giapintzakis, A. Salifoglou, *Inorg. Chem.* **2000**, *39*, 4044–4051.
[21] R. Bastian, R. Weberling, F. Palilla, *Anal. Chem.* **1956**, *28*, 459–462.
[22] a) P. O'Brien, H. Salacinski, M. Motevalli, *J. Am. Chem. Soc.* **1997**, *119*, 12695–12696; b) G. E. Hawkes, P. O'Brien, H. Salacinski, M. Motevalli, I. Abrahams, *Eur. J. Inorg. Chem.* **2001**, 1005–1011.
[23] J. Strouse, S. W. Layten, C. E. Strouse, *J. Am. Chem. Soc.* **1977**, *99*, 562–572.
[24] a) M. Matzapetakis, M. Dakanali, C. P. Raptopoulou, V. Tangoulis, A. Terkis, N. Moon, J. Giapintzakis, A. Salifoglou, *J. Biol. Inorg. Chem.* **2000**, *5*, 469–474; b) N. Kotsaskis, C. P. Raptopoulou, V. Tangoulis, A. Terkis, J. Giapintzakis, T. Jakusch, T. Kiss, A. Salifoglou, *Inorg. Chem.* **2003**, *42*, 22–31.
[25] I. Gautier-Luneau, F. Biaso, J.-L. Pierre, unpublished results.
[26] I. Gautier-Luneau, C. Fouquard, C. Merle, D. Luneau, J.-L. Pierre, *J. Chem. Soc. Dalton Trans.* **2001**, 2127–2131.
[27] a) A. Bodor, I. Banyai, L. Zekany, I. Toth, *Coord. Chem. Rev.* **2002**, *228*, 163–173; b) A. Bodor, I. Banyai, I. Toth, *Coord. Chem. Rev.* **2002**, *228*, 175–186.
[28] W. R. Harris, Z. Wang, Y. Z. Hamada, *Inorg. Chem.* **2003**, *42*, 3262–3273.
[29] a) T. L. Feng, P. L. Gurian, M. D. Healy, A. R. Barron, *Inorg. Chem.* **1990**, *29*, 408–411; b) S. A. Malone, P. Cooper, S. L. Heath, *J. Chem. Soc. Dalton Trans.* **2003**, 4572–4573.
[30] a) M. Grootveld, J. D. Bell, B. Halliwell, O. I. Aruoma, A. Bomford, P. J. Sadler, *J. Biol. Chem.* **1989**, *264*, 4417–4422; b) C. Hershko, G. Graham, G. W. Bates, E. A. Rachmilewitz, *Br. J. Haematol.* **1978**, *40*, 255–263.
[31] B. Faller, H. Nick, *J. Am. Chem. Soc.* **1994**, *116*, 3860–3865.
[32] D. A. Brown, K. M. Herlihy, S. K. O'Shea, *Inorg. Chem.* **1999**, *38*, 5198–5202.

Received: October 27, 2004
Published online: February 18, 2005

